

Modern Physics Letters A
 © World Scientific Publishing Company

REVIEW OF RECENT RESULTS FROM THE RHIC BEAM ENERGY SCAN

LOKESH KUMAR

*School of Physical Sciences, National Institute of Science Education and Research,
 Bhubaneswar, Odisha 751005, India*

lokesh@rcf.rhic.bnl.gov; lokesh@niser.ac.in

We review recent results from the RHIC beam energy scan (BES) program, aimed to study the Quantum Chromodynamics (QCD) phase diagram. The main goals are to search for the possible phase boundary, softening of equation of state or first order phase transition, and possible critical point. Phase-I of the BES program has recently concluded with data collection for Au+Au collisions at center-of-mass energies ($\sqrt{s_{NN}}$) of 7.7, 11.5, 19.6, 27, and 39 GeV. Several interesting results are observed for these lower energies where the net-baryon density is high at the mid-rapidity. These results indicate that the matter formed at lower energies (7.7 and 11.5 GeV) is hadron dominated and might not have undergone a phase transition. In addition, the centrality dependence of freeze-out parameters is observed for the first time at lower energies, slope of directed flow for (net)-protons measured versus rapidity shows an interesting behavior at lower energies, and higher moments of net-proton show deviation from Skellam expectations at lower energies. An outlook for the future BES Phase-II program is presented and efforts for the detailed study of QCD phase diagram are discussed.

Keywords: Quark Gluon Plasma; QCD phase diagram; QCD critical point; Phase transition; Chemical and Kinetic freeze-out; Directed and elliptic flow, dynamical charge correlations, Eccentricity, Nuclear modification factor.

PACS Nos.: 25.75.-q, 25.75.Nq, 12.38.Mh, 25.75.Dw, 25.75.Gz, 25.75.Ld

1. Introduction

The main goals of high-energy heavy-ion collision experiments are to search and study the hot and dense matter called Quark-Gluon Plasma (QGP) formed in these collisions¹. Moreover, there is a great interest in understanding the QCD phase diagram, a phase diagram for strong interactions, to the level of that for electromagnetic interactions such as water. The results from top RHIC energies suggest the formation of QGP¹. The focus has now shifted to study the QGP properties² and establish the QCD phase diagram. In this review, we will concentrate on the latter part which is establishing the QCD phase diagram through a dedicated program at RHIC called beam energy scan program^{3,4,5}. Figure 1 shows the schematic QCD phase diagram plotted as temperature T vs. baryonic chemical potential μ_B ⁶. There are two main phases predicted in the QCD phase diagram: QGP and hadronic

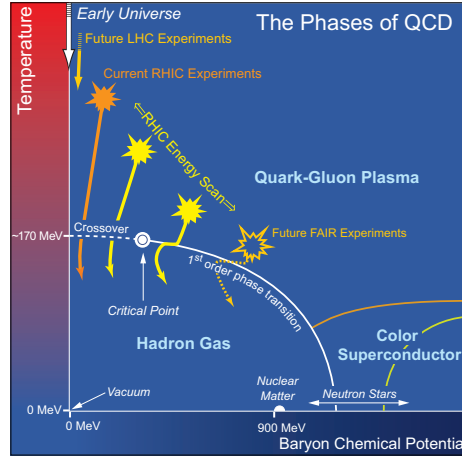


Fig. 1. (Color online) Schematic QCD phase diagram plotted as temperature T versus baryon chemical potential μ_B .

gas phase. Lattice QCD calculations predict that the transition between QGP and the hadronic gas at baryonic chemical potential $\mu_B = 0$ is a crossover⁷. At large μ_B , the transition between QGP and hadron gas is expected to be a first order phase transition^{8,9}. Subsequently, the end-point of this first-order phase transition line (while going towards the crossover) would be the position of a critical point¹⁰. While there is a little guidance from the theory side about the QCD phase diagram, efforts are ongoing from the experimental side to establish some of its distinct structures such as phase boundary between de-confined phase of quarks and gluons and hadron gas phase, first-order phase transition line, and the critical point.

Experimentally, the two axes: T and μ_B of the QCD phase diagram can be obtained from the momentum distributions and the ratios of the produced particles in heavy-ion collisions. Each collision energy corresponds to one T - μ_B point in the phase diagram. So, idea is to collect data at different center-of-mass energies by colliding heavy-ions. Once, the T - μ_B point is obtained, one can look at the various signatures for the phase boundary, first-order phase transition, and the critical point. One of the interesting aspect is to locate the energy where the established signatures of the QGP (at top RHIC energy) disappear or “turn-off”. This is how the RHIC beam energy scan program was planned^{3,4,5}. The proposal for the BES program was made in the year 2008. This was followed by a successful data taking and physics analysis of a test run of Au+Au collisions below injection energies at $\sqrt{s_{NN}} = 9.2$ GeV¹¹. The first phase of the BES program was started in the year 2010 with data taking in Au+Au collisions at three low energies of 7.7, 11.5, and 39 GeV. In 2011, two more energies at $\sqrt{s_{NN}} = 19.6$ and 27 GeV were included. Table 1 lists various

energies and corresponding number of events collected by the STAR detector in 2010–2011 for Phase-I of the BES program.

Table 1. The data collected during the Phase-I of the BES program.

| Year | $\sqrt{s_{NN}}$ (GeV) | N_{event} (Million) |
|------|-----------------------|------------------------------|
| 2010 | 7.7 | 5 |
| 2010 | 11.5 | 12 |
| 2010 | 39 | 130 |
| 2011 | 19.6 | 36 |
| 2011 | 27 | 70 |

This review is organized as follows. In Sec. 2, we discuss freeze-out parameters that provide information about T - μ_B points in the QCD phase diagram. In Sec. 3, signatures of first-order phase transition and that for turn-off of QGP are discussed. These include results on freeze-out eccentricity, directed flow, elliptic flow, dynamical charge correlations, and nuclear modification factor. The signatures for the search of possible critical point are discussed in Sec. 4 that include energy dependence of particle ratio fluctuations and higher moments of conserved quantities such as net-proton. Section 5 provides the outlook for the BES Phase-II program. Finally, we conclude with a summary in Sec. 6.

2. Freeze-out Parameters

The QCD phase diagram is the variation of temperature T and baryon chemical potential μ_B . These quantities can be extracted from the measured hadron yields. Transverse momentum spectra for the BES Phase-I energies are obtained for π , K , p , Λ , Ξ , K_S^0 , and ϕ ^{12,13}. From these distributions, corresponding particle yields are obtained and various particle ratios are constructed. These particle ratios are used to obtain the chemical freeze-out (a state after the collision when the yields of particles get fixed) conditions using the statistical thermal model (THERMUS)^{14,15,16}. The two main extracted parameters are chemical freeze-out temperature T_{ch} and μ_B . Figure 2 (left panel) shows the variation of the extracted chemical freeze-out parameters using the Grand-Canonical Ensemble (GCE) approach of THERMUS for different energies and centralities^{17,18}. The curves represent the parameterizations of T_{ch} and μ_B ^{19,20}. We observe that at top RHIC energy, there is a little variation of chemical freeze-out parameters with centrality. While at lower energies, T_{ch} shows a variation with μ_B as a function of centrality. The centrality dependence of these parameters is observed for the first time in heavy-ion collisions at these lower energies. One advantage of having such a dependence is that one can explore larger portion of the QCD phase diagram.

The particle spectra can be used to obtain the kinetic freeze-out (a state after the collision when the spectral shapes of particles get fixed) conditions using the Blast Wave (BW) model²¹. The BW model is used to simultaneously fit the π , K , p

4 Lokesh Kumar

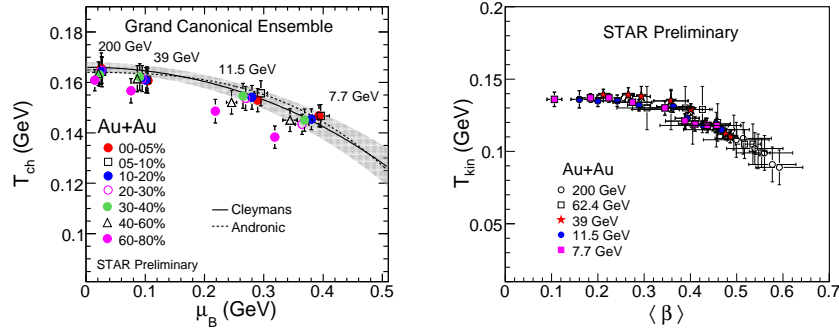


Fig. 2. (Color online) Left panel: Variation of T_{ch} with μ_B for different energies and centralities. Right panel: Variation of T_{kin} with $\langle\beta\rangle$ for different energies and centralities. Errors in both panels represent the quadrature sum of systematic and statistical errors.

spectra and the two main extracted parameters are kinetic freeze-out temperature T_{kin} and average flow velocity $\langle\beta\rangle$. Figure 2 (right panel) shows the variation of kinetic freeze-out parameters for different energies and centralities¹⁸. We observe that at a given collision energy, there is an anti-correlation between T_{kin} and $\langle\beta\rangle$. For a given collision centrality, the freeze-out temperature at high energy is lower and the average collectivity velocity $\langle\beta\rangle$ is larger due to expansion.

3. Search for First Order Phase Transition & Turn-off of QGP Signatures

Having discussed about accessing the QCD phase diagram by obtaining $T - \mu_B$ points, we can now discuss various signatures for first order phase transition or softest point in equation of state and those showing “turn-off” of QGP. These include freeze-out eccentricity, directed flow, elliptic flow, dynamical charge correlations, and nuclear modification factor.

3.1. Freeze-out Eccentricity

Eccentricity at freeze-out can be extracted as: $\epsilon_F = \frac{\sigma_y^2 - \sigma_x^2}{\sigma_y^2 + \sigma_x^2} \approx 2R_{s,2}^2/R_{s,0}^2$, where σ_x and σ_y correspond to the widths of the participant zone at freeze-out in the in-plane and out-of-plane directions, respectively²². $R_{s,2}^2$ and $R_{s,0}^2$ are the 2nd-order and 0th-order Fourier coefficients radius terms along the “side” direction (perpendicular to the direction of average transverse pair momentum or “out” and that along the beam direction or “long”), respectively. The ratio $R_{s,2}^2/R_{s,0}^2$ is less affected by flow so it carries mainly the geometric information. Freeze-out eccentricity may provide important information related to both the equation of state and dynamical processes involved in heavy-ion collisions as explained below. In non-central collisions, there is an initial anisotropy created (elliptic shape) that leads to more compres-

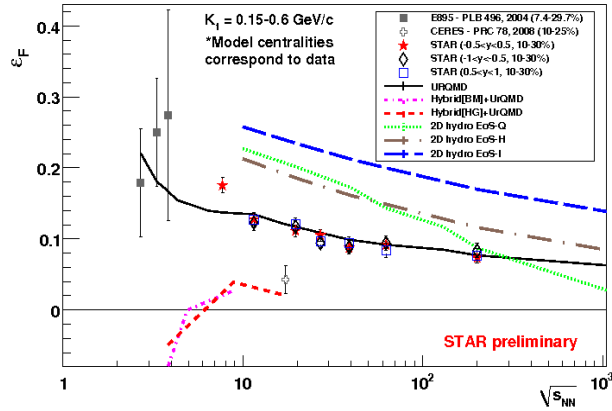


Fig. 3. (Color online) Freeze-out eccentricity as a function of beam energy compared to different model calculations.

sion along the shorter axis and hence larger initial pressure gradients. This might lead to expansion along the shorter axis thereby reducing the eccentricity. Ultimately, the system must evolve to a more round freeze-out shape. Increasing energy would lead to longer lifetimes and pressure gradients, and hence a monotonically decreasing excitation function for the freeze-out eccentricity would be expected. If the system undergoes a first-order phase transition, a mixed phase is expected. The system could spend more time in the mixed phase compared to that in other phases. This may lead to different expansions for different phases and hence non-monotonic freeze-out shape. Figure 3 shows the energy dependence of freeze-out eccentricity compared to several model calculations including UrQMD²³ and other 2D hydrodynamical models²⁴. These results suggest a monotonic decrease in the freeze-out eccentricity with beam energy.

3.2. Directed Flow

The directed flow v_1 is calculated as $\langle \cos(\phi - \Psi_1) \rangle$, where ϕ and Ψ_1 are the azimuthal angle of the produced particles and orientation of the first-order event plane, respectively. The directed flow measurements near midrapidity for protons are proposed to be sensitive to the equation of state (EOS)^{25,26,27}. It has been predicted that proton v_1 slope show a non-monotonic behavior as a function of beam energy illustrating change of sign from positive to negative at lower energies and again going back to positive at higher energies²⁷. This is sometimes called collapse of proton flow. The minimum in proton v_1 slope is proposed to correspond to a softest point in equation of state. Figure 4 shows the results from the beam energy scan. Plotted here is the v_1 slope (dv_1/dy' , where $y' = y/y_{\text{beam}}$ and y is rapidity), near midrapidity as a function of beam energy for the mid-central (10–40%) Au+Au collisions²⁸.

6 Lokesh Kumar

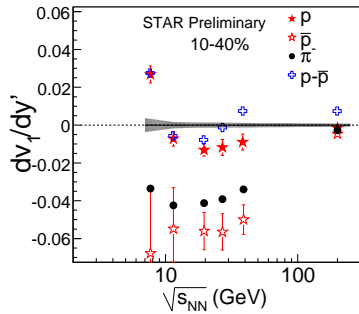


Fig. 4. (Color online) Directed flow slope (dv_1/dy' , $y'=y/y_{\text{beam}}$) for π^- , p , \bar{p} , and net-protons ($p-\bar{p}$) near midrapidity as a function of beam energy for mid-central (10–40%) Au+Au collisions. The shaded band refers to the systematic uncertainty on net-proton measurements.

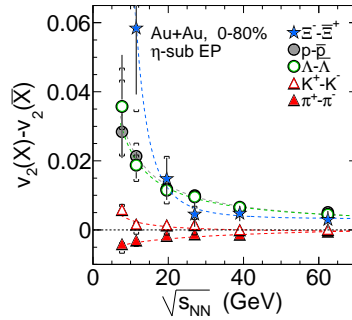


Fig. 5. (Color online) The difference in v_2 between particles and their corresponding anti-particles as a function of beam energy in 0–80% Au+Au collisions. The curves represent fits to data points as discussed in text. Both statistical (vertical lines) and systematic errors (caps) are shown.

The pion and anti-proton v_1 slopes show negative values for all the beam energies studied. The proton v_1 slope changes sign while going from 7.7 GeV to 11.5 GeV and then stays negative up to 200 GeV. However, the net-protons v_1 slope (obtained using v_1 slopes of p , \bar{p} and ratio of \bar{p}/p) changes sign from positive to negative and again becomes positive as a function of beam energy. Both proton and net-proton v_1 slopes show a dip (or minimum) around $\sqrt{s_{NN}} = 10\text{--}20$ GeV. In order to quantify the minimum position, it will be interesting to add one more energy point around 15 GeV. Also more theoretical as well as experimental studies are needed in order to understand these interesting observations.

3.3. Elliptic Flow

The elliptic flow v_2 is calculated as $\langle \cos 2(\phi - \Psi_2) \rangle$, where Ψ_2 is orientation of the second-order event plane. Elliptic flow mainly probes the early stages of heavy-ion collisions. At top RHIC energy of 200 GeV in Au+Au collisions, the elliptic flow scaled by the number of constituent quarks (n_q) versus $(m_T - m_0)/n_q$ (where $m_T = \sqrt{p_T^2 + m_0^2}$) shows a scaling behavior where mesons and baryons have similar values at intermediate p_T . This is referred to as the number of constituent quark (NCQ) scaling²⁹. It is an established signature of partonic matter formed in Au+Au collisions at 200 GeV and deviations from such scaling would indicate the dominance of hadronic interactions. Hence breaking of NCQ scaling at lower energies could be an indication of a “turn-off” of QGP signatures. Figure 5 shows the difference in v_2 of particles and corresponding anti-particles as a function of beam energy³⁰. The curves represent fits to data points with functional form: $f_{\Delta v_2}(\sqrt{s_{NN}}) = a\sqrt{s_{NN}}^{-b} + c$. The v_2 difference between particles and anti-particles is observed to increase when we go towards the lower energies. At low energies,

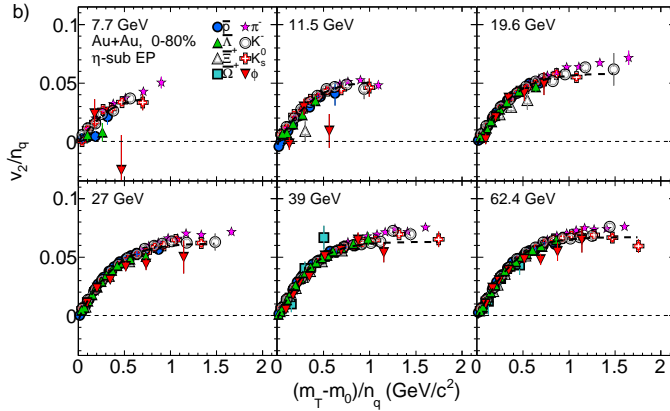


Fig. 6. (Color online) v_2/n_q as a function of $(m_T - m_0)/n_q$ for different particles in Au+Au collisions at $\sqrt{s_{NN}} = 7.7, 11.5, 19.6, 27, 39$ and 62.4 GeV. The errors shown are statistical only.

$v_2(\pi^-) > v_2(\pi^+)$, $v_2(K^+) > v_2(K^-)$, and $v_2(\text{baryons}) > v_2(\text{anti-baryons})$. This difference between particles and anti-particles suggests that the NCQ scaling among particles and anti-particles is broken. However, the observed difference between v_2 of particles and anti-particles could be qualitatively explained by the models incorporating baryon transport at midrapidity and hadronic interactions^{31,32}. We also observe that the baryons-mesons splitting for v_2 versus $m_T - m_0$ starts to disappear for anti-particles at 11.5 GeV and below. Figure 6 shows the v_2/n_q versus $(m_T - m_0)/n_q$ for different particles for $\sqrt{s_{NN}} = 7.7\text{--}62.4$ GeV³⁰. We observe that results for all the particles are consistent among each other within $\pm 10\%$ level, except for the ϕ -mesons at 7.7 and 11.5 GeV. At the largest $m_T - m_0$ the ϕ -meson data points deviate by 1.8σ and 2.3σ for $\sqrt{s_{NN}} = 7.7$ and 11.5 GeV, respectively. Since ϕ -mesons have smaller hadronic interaction cross-section, their smaller v_2 values could indicate that the hadronic interactions start to dominate over partonic effects for the systems formed at beam energies below $\sqrt{s_{NN}} = 11.5$ GeV^{33,34}. However, as can be seen from the figure, a higher statistics data are needed to extend the $m_T - m_0$ range and significance of the deviation observed.

3.4. Dynamical Charge Correlations

The dynamical charge correlations are studied through a three-particle mixed harmonics azimuthal correlator³⁵, $\gamma = \langle \cos(\phi_\alpha + \phi_\beta - 2\Psi_{RP}) \rangle$. This observable represents the difference between azimuthal correlations projected onto the direction of the angular momentum vector and correlations projected onto the collision reaction plane. It is suggested that the difference in the correlations between same sign and opposite sign charges in heavy-ion collisions could be related to local *parity* violation if there is a deconfinement and a chiral phase transition³⁶. This is also referred to

8 Lokesh Kumar

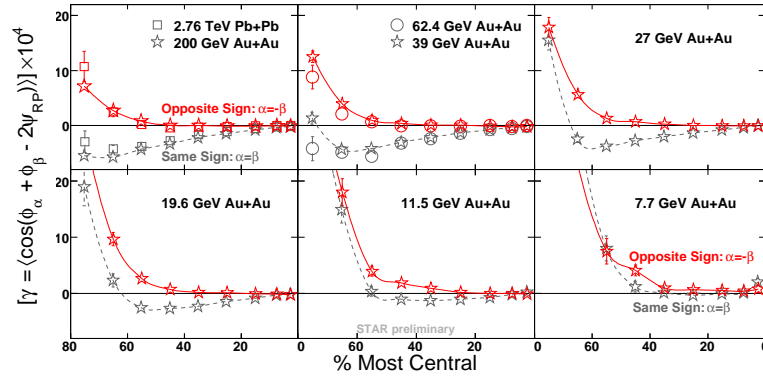


Fig. 7. (Color online) Dynamical charge correlations as a function of centrality for Au+Au collisions at $\sqrt{s_{NN}} = 7.7\text{--}200$ GeV. For comparison, results for Pb+Pb collisions at 2.76 TeV are also shown. Errors are statistical only.

as Chiral Magnetic Effect (CME). At top RHIC energies, we observed a separation between the correlations of same and opposite sign charges. If this difference can be attributed to the QCD phase transitions, the absence of such observation could be an indication of the system which did not undergo the phase transition. Hence, the observable could be useful to locate the energy in the BES program where the QGP signature “turns off”. Figure 7 shows the results for the beam energies from 7.7–200 GeV as a function of centrality³⁷. For comparison, Pb+Pb results from ALICE are also shown³⁸ which are observed to be consistent with the results from top RHIC energy. The separation between same and opposite sign charges decreases with decreasing energy and vanishes below $\sqrt{s_{NN}} = 11.5$ GeV.

3.5. Nuclear Modification Factor

Nuclear modification factor R_{CP} is one of the established observable for the signature of QGP at top RHIC energy³⁹. It is defined as ratio of yields at central collisions to those at peripheral collisions, scaled by the corresponding number of binary collisions N_{bin} . The number of binary collisions are calculated from the Monte Carlo model. It has been observed that at high p_T , the R_{CP} of various particles is less than unity³⁹, which is attributed to the energy loss of the partons in the dense medium. In the absence of dense medium, there may not be suppression of high p_T particles, which can serve as an indication of “turn-off” of a QGP signature.

Figure 8 (left panel) shows the R_{CP} of K_S^0 in Au+Au collisions at $\sqrt{s_{NN}} = 7.7\text{--}39$ GeV⁴⁰. We observe that for $p_T > 2$ GeV/c, the $R_{CP}(K_S^0)$ is less than unity at 39 GeV and then the value increases as the beam energy decreases. For $\sqrt{s_{NN}} < 19.6$ GeV, $R_{CP}(K_S^0)$ is above unity, indicating decreasing partonic effects at lower energies. Figure 8 (right panel) shows the R_{CP} results for charged hadrons in Au+Au collisions at $\sqrt{s_{NN}} = 7.7\text{--}200$ GeV⁴¹. Again, we observe no suppression at lower

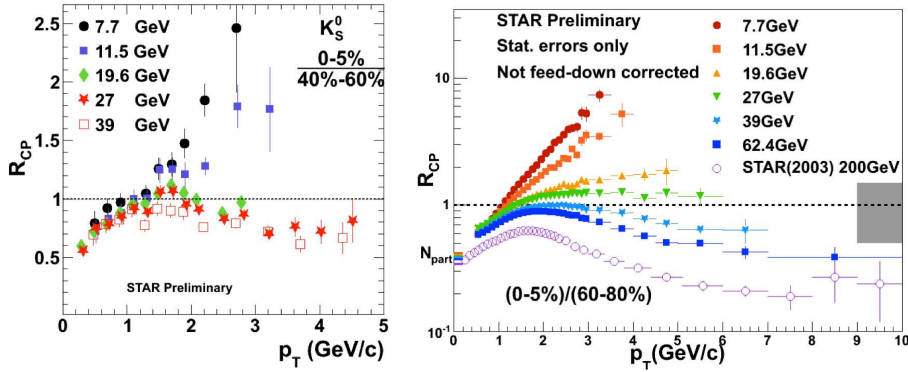


Fig. 8. (Color online) Left: $R_{CP} \left(\frac{0-5\%}{40\%-60\%} \right)$ for K_S^0 in Au+Au collisions at $\sqrt{s_{NN}} = 7.7-39$ GeV. Errors are statistical only. Right: $R_{CP} \left(\frac{0-5\%}{60\%-80\%} \right)$ for charged hadrons in Au+Au collisions at $\sqrt{s_{NN}} = 7.7-200$ GeV. Grey band corresponds to the systematic uncertainty.

energies for $p_T > 2$ GeV/c, supporting the $R_{CP}(K_S^0)$ results. Both results suggest that partonic effects become less important at lower energies and the cold nuclear matter effects (Cronin effect) start to dominate at these energies⁴².

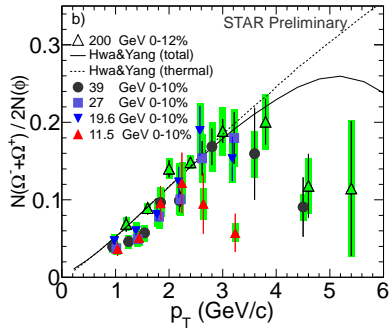


Fig. 9. (Color online) The baryon to meson ratio $N(\Omega^- + \Omega^+)/ (2N\phi)$ as a function of p_T in central Au+Au collisions at $\sqrt{s_{NN}} = 11.5-200$ GeV. The curves represent model calculations by Hwa and Yang for $\sqrt{s_{NN}} = 200$ GeV. Both statistical errors (vertical lines) and systematic errors (shaded bands) are shown.

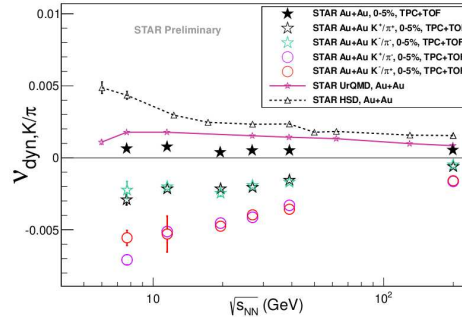


Fig. 10. (Color online) $\nu_{\text{dyn},K/\pi}$ for K/π (along with K^+/π^+ , K^-/π^- , K^+/π^- , and K^-/π^+) ratio in 0-5% central Au+Au collisions are shown as a function of energy. Results are compared with transport models such as UrQMD and HSD. Errors are statistical.

Figure 9 shows the baryon to meson ratio $N(\Omega^- + \Omega^+)/ (2N\phi)$ as a function of p_T in central Au+Au collisions at $\sqrt{s_{NN}} = 11.5-200$ GeV. The curves represent model calculations by Hwa and Yang in central collisions at $\sqrt{s_{NN}} = 200$ GeV^{43,44} which assume the Ω and ϕ yields to be generated from the recombination of thermal strange quarks having exponential p_T distribution. The particle ratio results at

$\sqrt{s_{NN}} = 19.6, 27,$ and 39 GeV seem to follow that of 200 GeV, indicating a maximum around $p_T \geq 3$ GeV/ c and then turning down as the p_T is increased. However, results at 11.5 GeV show different behavior i.e. show a maximum at somewhat lower p_T of ~ 2 GeV/ c before turning down for higher values of p_T . This observation suggests that there might be a significant change in the underlying p_T distributions of strange quarks recombining to form final Ω and ϕ for $\sqrt{s_{NN}} = 11.5$ GeV and those for $\sqrt{s_{NN}} \geq 19.6$ GeV.

4. Search for QCD Critical Point

In this section, we discuss the observables that could possibly be related to the critical point search. First, we discuss the particle ratio fluctuations such as K/π ratio fluctuations as a function of beam energy. After that, we discuss about the conserved number fluctuations that include net-proton higher moments results.

4.1. K/π Ratio Fluctuations

If a system passes close to a critical point, large density variations or enhanced fluctuations are expected e.g. as seen in critical opalescence. From experimental side, one expects a non-monotonic variation of a potential observable as a function of beam energy. Dynamical particle ratio fluctuations such as K/π , p/π , and K/p , might be sensitive to the initial state fluctuations arising from the existence of critical point^{45,46}. The observable used to quantify these (e.g. K/π) dynamical fluctuations ν_{dyn} is given by

$$\nu_{dyn,K/\pi} = \frac{\langle N_K(N_K - 1) \rangle}{\langle N_K \rangle^2} + \frac{\langle N_\pi(N_\pi - 1) \rangle}{\langle N_\pi \rangle^2} - 2 \frac{\langle N_K N_\pi \rangle}{\langle N_K \rangle \langle N_\pi \rangle}, \quad (1)$$

where N_K and N_π are the average number of kaons and pions in an event, respectively. For a pure Poisson distribution, $\nu_{dyn,K/\pi}$ will be zero. Figure 10 shows the ν_{dyn} results for K/π (along with K^+/π^+ , K^-/π^- , K^+/π^- , and K^-/π^+) ratio in 0–5% central collisions as a function of beam energy⁴⁷. The dynamical K/π ratio fluctuations show a smooth or monotonic behavior as a function of beam energy. The transport models such as HSD⁴⁸ and UrQMD²³ show a similar smooth dependence on beam energy as observed in data.

4.2. Conserved Number Fluctuations

Higher moments of conserved number fluctuations are proposed to be potential observables for the search of the critical point^{49,50,51}. For a static, infinite medium, the correlation length ξ diverges at critical point. The various moments of event-by-event conserved numbers (such as net-baryons, net-charge, and net-strangeness) distributions are related to different powers of the correlation length. Higher moments such as skewness S and kurtosis κ are related to higher power of the correlation length^{52,53}. Thus, these higher moments have a better sensitivity for the search of

the critical point. It has been proposed that the appropriate products of these moments such as $\kappa\sigma^2$ and $S\sigma$ can be related to the ratios of order susceptibilities calculated in lattice QCD and HRG model as $\kappa\sigma^2 = \chi_B^{(4)}/\chi_B^{(2)}$ and $S\sigma = \chi_B^{(3)}/\chi_B^{(2)}$ 54,55. One of the advantages of using these products or ratios is that they cancel the volume effects which are difficult to estimate in an experiment. So in this way, one can relate the experimental measurements with the lattice QCD observables for the search of critical point. Since in an experiment, it is difficult to obtain total baryons on an event-by-event basis, net-protons are used as a proxy for the net-baryons.

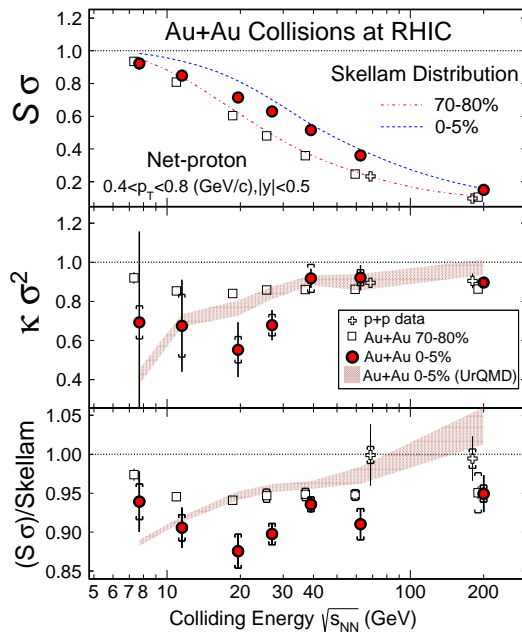


Fig. 11. (Color online) $\kappa\sigma^2$, $S\sigma$ and $S\sigma$ values normalized by the Skellam expectations as a function of collision energy and two different centralities. Results from $p + p$ collisions are also shown. All the results presented are corrected for detector efficiency. Results from UrQMD model calculations are also shown. The widths of bands represent statistical uncertainties. The error bars on data points are statistical while caps represent the systematic errors.

a smooth monotonic behavior as a function of collision energy. There are large uncertainties for data points below 19.6 GeV that call for higher statistics data at these energies. In addition, a direct comparison to QCD calculations with critical point obtained using similar dynamics at that of heavy-ion collisions can provide definite answer about the existence of critical point.

Figure 11 shows the $\kappa\sigma^2$ and $S\sigma$ for net-protons as a function of beam energy for different collision centralities 56,57. For comparison, the results are shown for Skellam expectations and UrQMD model calculations that do not include critical point 23. The results from $p + p$ collisions at 200 GeV are also shown. The bottom panel shows the $S\sigma$ values normalized by the corresponding Skellam expectations. We observe that the moment products $\kappa\sigma^2$ and $S\sigma$ show similar values for central for central 0-5% and peripheral collisions (70-80%) for $\sqrt{s_{NN}} = 39-200$ GeV. For beam energies below 39 GeV, they have different values for central and peripheral collisions. These values are below Skellam expectations for $\sqrt{s_{NN}} > 7.7$ GeV for 0-5% central collisions. The deviation from Skellam expectation is observed to be more significant at $\sqrt{s_{NN}} = 19.6$ and 27 GeV. The UrQMD model calculations show

5. BES Phase-II

The first phase of the BES program has yielded several promising results for the understanding of QCD phase diagram. Some of the observables require high statistics data to make definite statements. These include ϕ -meson v_2 to test the NCQ scaling hypothesis at lower energies and higher moments of net-protons to see whether there is a non-monotonic variation towards lower energies that could suggest a possible critical point. In addition, energy dependence of some observables suggest

Table 2. Proposed energies, μ_B values, and required number of events for the BES Phase-II. Also listed are the corresponding fixed target $\sqrt{s_{NN}}$, centre of mass rapidity, and μ_B reach.

| BES Phase - II | | | Fixed Target Collisions | | |
|-----------------------|---------------|------------------------------|-------------------------|-----------------|---------------|
| $\sqrt{s_{NN}}$ (GeV) | μ_B (MeV) | N_{event} (Million) | $\sqrt{s_{NN}}$ (GeV) | y_{CM} | μ_B (MeV) |
| 19.6 | 205 | 400 | 4.5 | 1.52 | 585 |
| 15 | 250 | 100 | 4.0 | 1.39 | 620 |
| 11.5 | 315 | 120 | 3.5 | 1.25 | 670 |
| 7.7 | 420 | 80 | 3.0 | 1.05 | 720 |

to have a need of one more energy point around 15 GeV. For example, proton and net-proton v_1 slopes suggest a minimum around 11.5–19.6 GeV as a function of energy which could be related to the softest point in equation of state. Having one more energy point in between would indicate the exact location of the minimum. Similar reason (although there is a monotonic variation as a function of beam energy at the moment) might be argued for the freeze-out eccentricity. For net-proton higher moments, adding 15 GeV along with high-statistics data at lower energies might provide the clear energy dependence trend with high significance. One more energy point at 15 GeV is also important in view of the fact that the gap between 11.5 and 19.6 GeV in terms of μ_B is more than 100 MeV.

For the reasons mentioned above, RHIC has decided to continue the exploration of QCD phase diagram and hence proposed a second phase of the BES program. The proposal for BES Phase-II includes high statistics data below 20 GeV as listed in

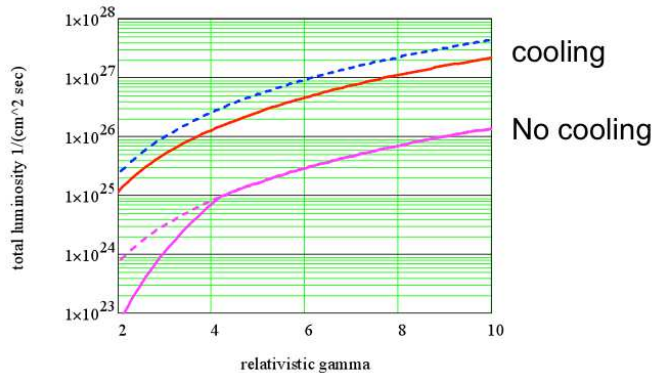


Fig. 12. (Color online) Improvement in RHIC luminosity for the lower energies with electron cooling and long bunches (with space charge tune spread $\Delta Q_{\text{SC}} = 0.05$ and $\sigma_s = 3$ m.)

the Table 2. To achieve the high statistics data at lower energies, an electron cooling device is requested to be installed at RHIC for increasing the beam luminosity⁵⁸. Simulation results (see Fig. 12) indicate that with electron cooling, a significant improvement can be made to increase luminosity (as shown by red solid curve in the figure). An additional improvement in luminosity (as shown by blue dashed curve) may be possible by operating with longer bunches at the space-charge limit in the collider⁵⁹. Electron cooling may increase the luminosity by a factor of 3–10 and with longer bunches the luminosity may be increased by another factor of 2–5. The high statistics data from BES Phase-II will not only allow the precision measurements of the important observables discussed here but will also be helpful in the measurements of rare probes such as dilepton production and hypertriton measurements at lower energies^{60,61}.

To maximize the use of collisions provided at STAR, a fixed target proposal is made along with BES Phase-II. The idea is to install a fixed Au target inside the STAR beam pipe to perform the Au(beam)-Au(target) collisions. Such collisions will provide lower reach for the center of mass energies and higher reach for the μ_B values for a given BES Phase-II energy. The beam energies and the μ_B values for the fixed target collisions are listed in the Table 2 corresponding to the proposed BES Phase-II energies. The μ_B values are obtained from the parameterizations in Ref. ²⁰. Clearly, it provides an opportunity to reach the large values of μ_B and hence to explore the larger portion of the QCD phase diagram. One of the advantages for such a proposal is that the data taking for these fixed target collisions can be done concurrently during the normal RHIC running and hence it will not affect the normal RHIC operations.

These programs will also benefit from the proposed inner sector upgrade of STAR TPC called the iTPC upgrade⁶². At the moment, inner sector of the TPC has the following issues: the inner sector wires are showing the signs of ageing and unlike the outer TPC sectors, it does not have the hermetic coverage at all radii. The spacing between the rows is greater than 5 cm which results in missing rows. To overcome these issues, it has been proposed to increase the segmentation on the inner pad plane and renew the inner sector wires. Simulation studies suggest that with iTPC upgrade it is possible obtain better momentum resolution, better dE/dx resolution for particle identification, and improved acceptance at higher pseudorapidity η and low p_T . At the moment, TPC η coverage is about $|\eta| < 1.0$, however, with iTPC upgrade, it might reach $|\eta| < 1.7$. Similarly, lowest p_T achieved can be as low as 60 MeV/ c compared to the present value of 125 MeV/ c . The above listed improvements will definitely strengthen the technical aspects in the Physics analyses proposed for the BES Phase-II. The BES Phase-II is expected to start around 2018-2019.

6. Summary

The BES Phase-I enables RHIC to cover large range of μ_B (20–400 MeV) in the phase diagram. At lower energies, a centrality dependence of freeze-out parameters

is observed. The observables such elliptic flow v_2 , nuclear modification factor R_{CP} , baryon to meson ratio Ω/ϕ , dynamical charge correlations, suggest that hadronic interactions dominate for $\sqrt{s_{NN}} \leq 11.5$ GeV or that the system did not undergo QGP phase transition at these lower energies. The (net)-proton directed flow v_1 slope show interesting behavior for the energy range $\sqrt{s_{NN}} < 20$ GeV. The proton v_1 slope changes sign between 7.7 and 11.5 GeV. The net-proton v_1 slope changes sign twice as a function of beam energy. Both proton and net- proton v_1 slopes show a minimum around 11.5–19.6 GeV. The $\kappa\sigma^2$ and $S\sigma$ for net-protons show most significant deviations from Skellam expectations at $\sqrt{s_{NN}} = 19.6$ and 27 GeV. BES Phase-II along with electron cooling, fixed target proposal, and iTPC upgrade provides optimistic future for the exploration of the QCD phase diagram, and hence for critical point and phase boundary search.

We thank Prof. D. Keane, Prof. B. Mohanty, and Prof. Nu Xu for reading the manuscript and providing helpful comments and suggestions.

References

1. J. Adams *et al.* (STAR Collaboration), Nucl. Phys. A **757**, 28 (2005).
2. V. Roy, A. K. Chaudhuri and B. Mohanty, Phys. Rev. C **86**, 014902 (2012).
3. M. M. Aggarwal *et al.* (STAR Collaboration), arXiv:1007.2613.
4. L. Kumar (for STAR Collaboration), Nucl. Phys. A **862**, 125 (2011);
5. B. Mohanty, Nucl. Phys. A **830**, 899C (2009).
6. USA-NSAC 2007, Long range plan.
7. Y. Aoki, G. Endroli, Z. Fodor, S. D. Katz and K. K. Szabo, Nature **443** 675, (2006).
8. S. Ejiri, Phys. Rev. D **78**, 074507 (2008).
9. E. S. Bowman and J. I. Kapusta, Phys. Rev. C **79**, 015202 (2009).
10. M. A. Stephanov, Prog. Theor. Phys. Suppl. **153**, 139 (2004) [Int. J. Mod. Phys. A **20**, 4387 (2005)] [hep-ph/0402115].
11. B. I. Abelev *et al.* (STAR Collaboration), Phys. Rev. C **81**, 024911 (2010).
12. L. Kumar (for STAR Collaboration), J. Phys. G: Nucl. Part. Phys. **38**, 124145 (2011);
13. X. Zhu (for STAR Collaboration), Acta Phys. Polon. B Proc. Supp. **5**, 213 (2012).
14. J. Adams *et al.* (STAR Collaboration), Nucl. Phys. A **757**, 102 (2005);
15. A. Andronic, F. Beutler, P. Braun-Munzinger, K. Redlich and J. Stachel, Phys. Lett. B **675**, 312 (2009) [arXiv:0804.4132 [hep-ph]].
16. S. Wheaton and J. Cleymans, Comput. Phys. Commun. **180**, 84 (2009) [hep-ph/0407174].
17. L. Kumar [STAR Collaboration], Nucl. Phys. A **904-905**, no. issue, 256c (2013) [arXiv:1211.1350 [nucl-ex]].
18. S. Das [STAR Collaboration], Nucl. Phys. A **904-905**, 891c (2013) [arXiv:1210.6099 [nucl-ex]].
19. A. Andronic, P. Braun-Munzinger and J. Stachel, Nucl. Phys. A **834**, 237C (2010) [arXiv:0911.4931 [nucl-th]].
20. J. Cleymans, H. Oeschler, K. Redlich and S. Wheaton, Phys. Rev. C **73**, 034905 (2006) [hep-ph/0511094].
21. E. Schnedermann, J. Sollfrank and U. W. Heinz, Phys. Rev. C **48**, 2462 (1993) [nucl-th/9307020].
22. E. Mount, G. Graef, M. Mitrovski, M. Bleicher and M. A. Lisa, Phys. Rev. C **84**, 014908 (2011) [arXiv:1012.5941 [nucl-th]].

23. M. Bleicher, E. Zabrodin, C. Spieles, S. A. Bass, C. Ernst, S. Soff, L. Bravina and M. Belkacem *et al.*, J. Phys. G **25**, 1859 (1999) [hep-ph/9909407].
24. M. A. Lisa, E. Frodermann, G. Graef, M. Mitrovski, E. Mount, H. Petersen and M. Bleicher, New J. Phys. **13**, 065006 (2011) [arXiv:1104.5267 [nucl-th]].
25. J. Brachmann, S. Soff, A. Dumitru, H. Stoecker, J. A. Maruhn, W. Greiner, L. V. Bravina and D. H. Rischke, Phys. Rev. C **61**, 024909 (2000) [nucl-th/9908010].
26. L. P. Csernai and D. Rohrlich, Phys. Lett. B **458**, 454 (1999) [nucl-th/9908034].
27. H. Stoecker, Nucl. Phys. A **750**, 121 (2005) [nucl-th/0406018].
28. Y. Pandit [STAR Collaboration], Nucl. Phys. A **904-905**, 357c (2013). [arXiv:1210.5315 [nucl-ex]].
29. J. Adams *et al.* (STAR Collaboration), Phys. Rev. Lett. **95**, 122301 (2005).
30. L. Adamczyk *et al.* (STAR Collaboration), Phys. Rev. Lett. **110**, 0142301 (2013).
31. J. C. Dunlop, M. A. Lisa and P. Sorensen, Phys. Rev. C **84**, 044914 (2011) [arXiv:1107.3078 [hep-ph]].
32. J. Xu, L. -W. Chen, C. M. Ko and Z. -W. Lin, Phys. Rev. C **85**, 041901 (2012) [arXiv:1201.3391 [nucl-th]].
33. B. Mohanty and N. Xu, J. Phys. G **36**, 064022 (2009).
34. M. Nasim, B. Mohanty and N. Xu, Phys. Rev. C **87**, 014903 (2013).
35. B. I. Abelev *et al.* (STAR Collaboration), Phys. Rev. Lett. **103**, 251601 (2009).
36. K. Fukushima, D. E. Kharzeev and H. J. Warringa, Phys. Rev. D **78**, 074033 (2008) [arXiv:0808.3382 [hep-ph]].
37. G. Wang (for STAR Collaboration), Nucl. Phys. A **904-905**, 248c (2013).
38. B. Abelev *et al.* [ALICE Collaboration], Phys. Rev. Lett. **110**, 012301 (2013) [arXiv:1207.0900 [nucl-ex]].
39. M. A. C. Lamont (for the STAR Collaboration), J. Phys. Conf. Ser. **50**, 192 (2006).
40. X. Zhang (for STAR Collaboration), Nucl. Phys. A **904-905**, 543c (2013).
41. E. Sangaline (for STAR Collaboration), Nucl. Phys. A **904-905**, 771c (2013).
42. J. W. Cronin, H. J. Frisch, M. J. Shochet, J. P. Boymond, R. Mermod, P. A. Piroué and R. L. Sumner, Phys. Rev. D **11** (1975) 3105.
43. R. C. Hwa and C. B. Yang, Phys. Rev. C **75**, 054904 (2007) [nucl-th/0602024].
44. R. C. Hwa and C. B. Yang, Phys. Rev. C **66**, 025205 (2002) [hep-ph/0204289].
45. C. Pruneau, S. Gavin, and S. Voloshin, Phys. Rev. C **66**, 044904 (2002).
46. J. Adams *et al.* (STAR Collaboration), Phys. Rev. C **68**, 044905 (2003).
47. P. Tribedy (for STAR Collaboration), Nucl. Phys. A **904-905**, 463c (2013).
48. M. I. Gorenstein, M. Hauer, V. P. Konchakovski and E. L. Bratkovskaya, Phys. Rev. C **79**, 024907 (2009) [arXiv:0811.3089 [nucl-th]].
49. M. M. Aggarwal *et al.* (STAR Collaboration), Phys. Rev. Lett. **105**, 022302 (2010) [arXiv:1004.4959 [nucl-ex]].
50. S. Gupta, X. Luo, B. Mohanty, H. G. Ritter and N. Xu, Science **332**, 1525 (2011) [arXiv:1105.3934 [hep-ph]].
51. F. Karsch and K. Redlich, Phys. Lett. B **695**, 136 (2011).
52. M. A. Stephanov, Phys. Rev. Lett. **102**, 032301 (2009);
53. M. A. Stephanov, Phys. Rev. Lett. **107**, 052301 (2011).
54. R. V. Gavai and S. Gupta, Phys. Lett. B **696**, 459 (2011) [arXiv:1001.3796 [hep-lat]].
55. M. Cheng, P. Hendge, C. Jung, F. Karsch, O. Kaczmarek, E. Laermann, R. D. Mawhinney and C. Miao *et al.*, Phys. Rev. D **79**, 074505 (2009) [arXiv:0811.1006 [hep-lat]].
56. X. Luo (for STAR Collaboration), Nucl. Phys. A **904-905**, 911c (2013).
57. L. Adamczyk *et al.* (STAR Collaboration), arXiv:1309.5681.
58. A. Fedotov, and W. Fischer, Private communications, 2012.
59. A. Fedotov and M. Blaskiewicz, BNL CAD Tech Note: C-A/AP/449 (February 10,

16 *Lokesh Kumar*

2012).

60. B. Huang (for STAR Collaboration), Nucl. Phys. A **904-905**, 565c (2013).
61. Y. Zhu (for STAR Collaboration), Nucl. Phys. A **904-905**, 551c (2013).
62. Y. Xu (for STAR Collaboration), poster “Inner TPC Upgrade at STAR”, 2013 RHIC & AGS Annual Users Meeting, BNL, USA.